energies

MDPI

Article

Application of a $LiFePO_4$ Battery Energy Storage System to Primary Frequency Control: Simulations and Experimental Results

Fabio Massimo Gatta [1], Alberto Geri [1], Regina Lamedica [1], Stefano Lauria [1], Marco Maccioni [1,*], Francesco Palone [2], Massimo Rebolini [2] and Alessandro Ruvio [1]

[1] Department of Astronautics, Electric and Energy Engineering, Sapienza University of Rome, Rome 00184, Italy; fabiomassimo.gatta@uniroma1.it (F.M.G.); alberto.geri@uniroma1.it (A.G.); regina.lamedica@uniroma1.it (R.L.); stefano.lauria@uniroma1.it (S.L.); alessandro.ruvio@uniroma1.it (A.R.)

[2] Terna S.p.A., Rome 00156, Italy; francesco.palone@terna.it (F.P.); massimo.rebolini@terna.it (M.R.)

* Correspondence: marco.maccioni@uniroma1.it; Tel.: +39-06-44585540

Academic Editor: Peter J. S. Foot

Received: 29 July 2016; Accepted: 25 October 2016; Published: 29 October 2016

Abstract: This paper presents an experimental application of $LiFePO_4$ battery energy storage systems (BESSs) to primary frequency control, currently being performed by Terna, the Italian transmission system operator (TSO). BESS performance in the primary frequency control role was evaluated by means of a simplified electrical-thermal circuit model, taking into account also the BESS auxiliary consumptions, coupled with a cycle-life model, in order to assess the expected life of the BESS. Numerical simulations have been carried out considering the system response to real frequency measurements taken in Italy, spanning a whole year; a parametric study taking into account different values of governor droop and of BESS charge/discharge rates (*C-rates*) was also performed. Simulations, fully validated by experimental results obtained thus far, evidenced a severe trade-off between expected lifetime and overall efficiency, which significantly restricts the choice of operating parameters for frequency control.

Keywords: battery energy storage system (BESS); $LiFePO_4$ battery; primary frequency control

1. Introduction

The "smart grid" paradigm envisages a massive presence of non-programmable renewable energy sources: in this context, battery energy storage systems (BESSs) are liable to play a key role at both distribution and transmission level, given their potential ability to fulfill roles such as load shifting, peak shaving, frequency and also voltage control [1–6]. Moreover, BESSs have also been proposed in integration to electric power systems supplying traction and mobility systems, with the aim to maximize the energy efficiency [7–10]. In principle, the study of BESS impact on the electric power system should include environmental aspects, optimal siting, as well as power quality issues and harmonic disturbances, in accordance with existing standards [11–18]. Generally speaking, technical features such as battery size (in terms of both rated power and energy), efficiency, transient performance, cycling and lifetime depend on the specific application. In order to evaluate the economic return of each application, local energy market rules must be taken into account.

This paper deals with the application of a BESS based on lithium iron phosphate ($LiFePO_4$) batteries to primary frequency control (PFC). Since conventional power plants are increasingly displaced by (mostly non-dispatchable) generation from renewable energy sources, transmission system operators (TSOs) are looking for new PFC providers to preserve frequency quality. Li-ion BESSs are being evaluated for the PFC role [19,20], which entails exacting requirements such as fast response, high number of charge/discharge cycles and wide depth-of-discharge (*DOD*); notably, $LiFePO_4$

batteries look very promising, due to their chemical and thermal stability which could ensure a long lifetime under the PFC cycling conditions at a relatively low cost [21–23].

However, to date there is not enough operating experience confirming the PFC applicability and the performances (expected lifetime, round trip efficiency) of $LiFePO_4$ batteries. To this end, a coupled electrical-thermal model of a $LiFePO_4$ battery has been developed and validated against experimental tests by Terna (the Italian TSO). The model has been used to simulate PFC operation of a 1-MW/1-MWh $LiFePO_4$ BESS deployed by Terna, considering different values of droop and discharge rate (*C-rate*). The paper is organized as follows. Section 2 briefly recalls the Terna experimental BESS system, while Section 3 details the proposed PFC application. Section 4 deals with BESS modelling; experimental test results are shown in Section 5 and PFC simulation results are reported in Section 6.

2. The Terna Experimental $LiFePO_4$ Battery Energy Storage System

There are a significant number of manufacturers of $LiFePO_4$ batteries, since they use readily available raw materials and are thermally and chemically stable, thus ensuring safety as well as long service life. Moreover, the high power-to-energy ratio makes $LiFePO_4$ batteries attractive for BESS applications. $LiFePO_4$ have a lower nominal cell voltage (3.2 V) than other Li-ion batteries. The normal voltage for grid (stationary) application ranges between 2.8 and 3.6 V, in order to increase battery life avoiding operation at extreme values of the state-of-charge (SOC) near full charge or full discharge. The maximum continuous discharge rate of presently available MWh-sized systems can vary from 0.2C [19] to 4C [20], depending on the manufacturing technology and module thermal design. *C-rate* range requirements vary widely with the specific application: renewable energy sources balancing typically requires *C-rates* ranging between 0.2C and 1C, whereas PFC might involve *C-rates* ranging between 1C and 4C. Several $LiFePO_4$ BESS projects have been recently commissioned in China, America and Europe; in Italy, two $LiFePO_4$ systems have been recently installed by Terna as part of the wider "Storage Lab" [24,25] experimental BESS project. Terna's $LiFePO_4$ BESS is based on prismatic cells (Figure 1) suitable for stationary applications, located in an aluminum case.

Figure 1. Prismatic $LiFePO_4$ cells.

The series connection of four such cells forms a battery module with a 12.8 V-2.37 kWh rating. The battery module is sealed to prevent moisture ingress and to avoid leaks in case of battery failure: as a consequence, the thermal behavior of the cells inside the module differs substantially from that of free-standing cells. Each module is provided with its own battery management system (BMS) for cell balancing and battery monitoring. Modules are series-connected to form battery strings (mounted on racks designed with sufficient spacing for proper ventilation and cooling [24]), which are paralleled inside the air-conditioned battery container (Figure 2). Each of Terna's 1 MW/1 MWh BESS includes a battery container and a dual-stage power conditioning system (PCS) [26]. The PCS is connected from the low voltage (LV) level to a 20 kV medium voltage (MV) busbar via an integrated MV/LV transformer; the whole system is in turn connected to the Terna 150 kV high voltage (HV) sub-transmission network through a HV/MV transformer.

Extensive testing was carried out on the above described $LiFePO_4$ batteries, focusing on safety requirements [27–29] and battery performance. The latter tests involved intensive cycling of single battery modules (12.8 V-185 Ah) and performance tests on battery string specimens (256 V-185 Ah),

with the aim of verifying the expected battery life in normal operation. Moreover, PFC performance was evaluated by cycling a string specimen with a power profile emulating the response of a virtual governor to an actual ENTSO-E (acronym for European Network of Transmission System Operators for Electricity) measured frequency pattern.

Figure 2. Racks for battery strings, installed inside an air-conditioned cabinet.

The experimental setup included an electronic variable load (model ZS4206, H&H, Konzell, Germany), a controllable dc power supply (SM 15-400, Delta Elektronika, Zierikzee, Netherlands) and a measurement/monitoring system (cFP2220, cFP-AI-118, cFP-TC-120, National Instruments, Austin, TX, USA). This allowed to measure fundamental battery state variables such as current, individual cell voltages and temperatures, subsequently used to estimate battery parameters (resistance, thermal inertia) and performances (round-trip efficiency, battery life). Given the modular design of the BESS, results of tests performed on individual battery strings can be straightforwardly extended to the whole 1 MW/1 MWh system.

3. Application of the $LiFePO_4$ Battery Energy Storage System to Primary Frequency Control

3.1. Short Review of Battery Energy Storage System Applications to Primary Frequency Control

PFC is the most important task for the stability of the electrical power system. The first utility-scale BESS (based on lead-acid batteries) in Europe used for PFC was deployed in the 1980s in West Berlin [30], where for political reasons the supply system was not connected to the East Germany's national grid. Another relevant PFC application is the 1 MW Li-ion BESS operated by Elektrizitätswerke des Kantons Zürich (EKZ), the Canton of Zürich utility, in Dietikon, Switzerland [31]. Three applications (PFC, peak shaving and islanded operation) of the BESS are discussed and preliminary results regarding PFC application are supplied, showing the suitability of BESS for such tasks. Finally, many large-scale projects involving BESSs for PFC application have been recently deployed: these are recorded in the US Department of Energy database, together with hundreds projects involving other applications [32].

3.2. Primary Frequency Control in the ENTSO-E European Synchronous System

ENTSO-E is the association of 41 TSOs from 34 countries in Europe, accounting for three interconnections (namely the continental synchronous power system which links most European countries, plus the "Nordic" and "Baltic" interconnections), as well as the British—Irish and Sardinia—Corsica asynchronous power systems. The Continental Europe Operation Handbook [33] summarizes technical requirements and procedures for operation, control and security of the "continental" grid, in which frequency control (primary, secondary and tertiary control) obviously plays a paramount role. In particular, primary frequency control "[. . .] stabilizes the system frequency at a

stationary value after a disturbance or incident in the time-frame of seconds" [33]. PFC is carried out by proportional regulators, so that a quasi-steady-state frequency deviation Δf (defined as $\Delta f = f - f_n$, being f_n the nominal frequency of the interconnected grid), caused by an unbalance ΔP_a between demand and generation, will cause all generators participating in PFC to change their output according to the Equation (1):

$$\Delta P_G = -\frac{\Delta f}{f_n} \cdot \frac{P_{Gn}}{s} \cdot 100, \quad (1)$$

where ΔP_G (MW) is the variation of the active power output of the generation unit, P_{Gn} (MW) is the rated active power output of the generation unit and s (%) is the governor droop. No change in output is required if Δf does not exceed ± 10 mHz, to cater for the combined effects of frequency response insensitivity and governor dead band. Terna mandates 4% droop for hydroelectric and 5% droop for thermal power plants, respectively [34], whereas no prescription regarding BESSs is reported at present (2016).

3.3. Frequency Profile Used in Simulations

The PFC tests were carried out offline, by feeding the PCS of a 50 kW–50 kWh battery string (20 series-connected modules) with a power command directly proportional to a frequency deviation signal obtained from the actual ENTSO-E real-time frequency recording for the year 2014, in accordance with the pseudo-steady-state control characteristic (1). Frequency was sampled at 1-s intervals; the droop of the equivalent governor was taken at 0.5%, resulting in a λ = 200 kW/Hz power-frequency characteristic given the *C-rate* 1C. Offline testing was justified by the negligible influence of the test specimen on the overall Italian contribution to European primary frequency control.

Figure 3a shows the frequency vs. time for a random day (the ± 10 mHz insensitivity/dead-band window is also shown), whereas Figure 3b reports the probability distribution of recorded frequency values during the whole year: the maximum and minimum recorded values were 50.12 Hz and 49.89 Hz, respectively [35].

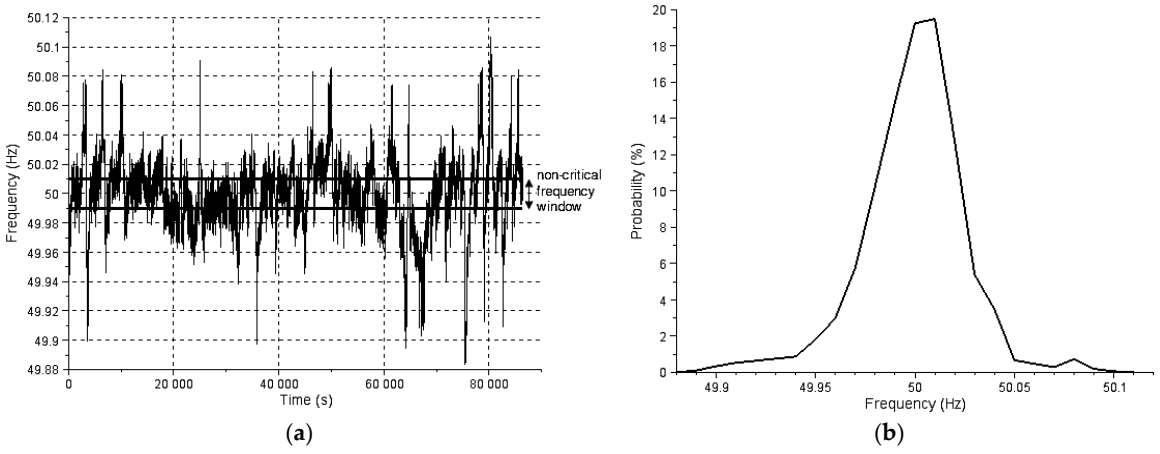

Figure 3. Italian (ENTSO-E) frequency profile measured by Terna and used in PFC tests: (**a**) frequency vs. time during one day; and (**b**) probability distribution of the whole yearly power frequency recording.

4. Battery Energy Storage System Modelling

The model adopted for simulating the $LiFePO_4$ BESS consists of a coupled electrical-thermal model for a battery string, plus a "lifetime" (aging) model to take into account the long-term battery loss of capacity. Validation of the electrical-thermal model, when used in in PFC simulations, against experimental tests by Terna is reported in Section 5.

4.1. The Electrical-Thermal Model

The battery itself is simulated by a coupled electrical-thermal model. The electrical part, shown in Figure 4, is an equivalent Thévenin circuit consisting of a voltage generator, E_m, in series with a single resistance, R_0. The value of the no-load voltage E_m has been taken as a function of SOC, but not of battery temperature T. In fact, during tests performed by Terna with s = 0.5% and *C-rate* = 1C, battery temperature was almost stable at around 25 °C; moreover, the effect of T on no-load voltage is not significant in the operating range (from 20 to 55 °C), as shown in [36]. Battery resistance R_0 has been assumed to depend on SOC and battery temperature but not on time, i.e., the effect on R_0 of battery ageing due to cycling has been neglected. Note that R_0 takes different values, depending on whether the battery is charging, $R_{0,c}$(SOC,T), or discharging, $R_{0,d}$(SOC,T). The resulting circuit can be regarded as a simplification of the detailed electrical model in [37], which includes an additional shunt-connected voltage generator E_p in series with an impedance Z_p, accounting for parasitic effects, as well as a number of *R-C* parallel blocks in series with R_0 in order to take into account the dynamic behavior of the battery. Model simplifications (e.g., removal of the shunt parasitic branch) are partly due to uncertainty of battery parameters and lack of data; moreover, the analysis of Terna experimental data suggests that, at least for the PFC-oriented simulations of the paper, the suppression of the *R-C* parallel blocks does not substantially decrease model performance. The latter remark also applies to the dependence of R_0 on load current (evidenced for instance in [38,39]), which has been disregarded.

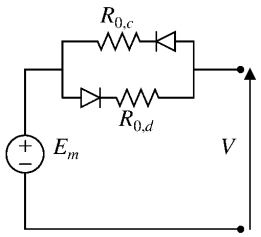

Figure 4. Simplified Thévenin equivalent circuit model of the battery (see text for details).

Figure 5a reports the measured values of the no-load voltage E_m as a function of SOC, yielded by Terna tests on a real $LiFePO_4$ battery (with T constant at 25 °C), as well as the curve used in the model of Figure 4. $R_{0,c}$(SOC,T) and $R_{0,d}$(SOC,T) values, respectively measured during charge and discharge duty, are shown in Figure 5b, which also includes values used in the simulation model. Terna also performed experimental tests to assess the dependence of both $R_{0,c}$ and $R_{0,d}$ on temperature.

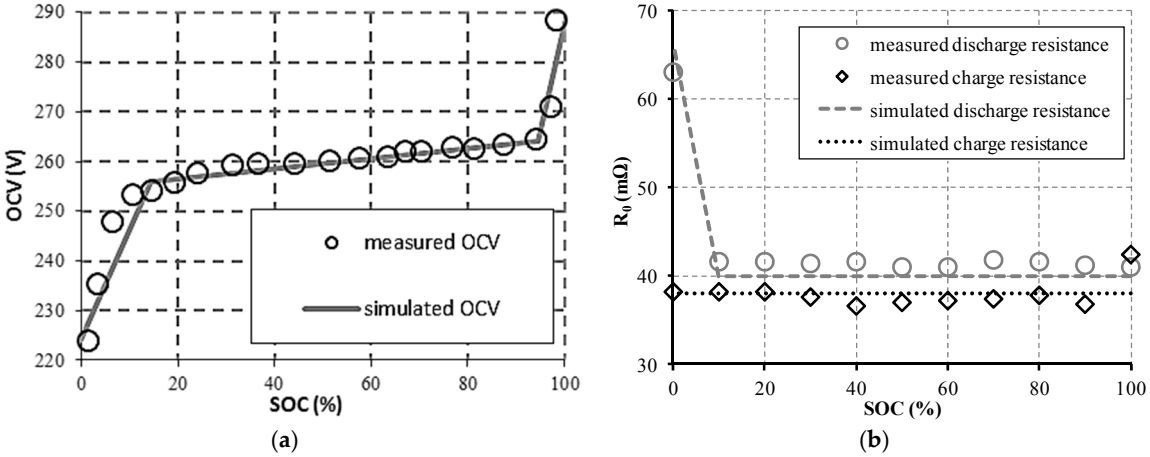

Figure 5. Measured and simulated parameter values for the Figure 4 model, as a function of state-of-charge (SOC). (**a**) No-load voltage E_m; and (**b**) charge and discharge resistances $R_{0,c}$ and $R_{0,d}$.

1-min/23 A current steps (corresponding to a *C-rate* equal to 0.125C) was impressed, measuring $R_{0,c}$ and $R_{0,d}$ for three different temperatures (20 °C, 30 °C, 40 °C) and three different SOC values (10%, 50%, 90%). Tables 1 and 2 report test results for $R_{0,d}$ and $R_{0,c}$, respectively.

Table 1. Battery discharge resistances measured for different SOC values and temperatures.

$R_{0,d}$ at SOC 10% (Ω)	$R_{0,d}$ at SOC 50% (Ω)	$R_{0,d}$ at SOC 90% (Ω)	Temperature (°C)
0.0399	0.0407	0.0374	20
0.0365	0.0348	0.0341	30
0.0307	0.0323	0.0306	40

Table 2. Battery charge resistances measured for different SOC values and temperatures.

$R_{0,c}$ at SOC 10% (Ω)	$R_{0,c}$ at SOC 50% (Ω)	$R_{0,c}$ at SOC 90% (Ω)	Temperature (°C)
0.0377	0.0393	0.0402	20
0.0335	0.0359	0.0352	30
0.0309	0.0310	0.0301	40

Based on such results, the dependence of $R_{0,c}$ and $R_{0,d}$ on temperature has been taken as linear in the operating range (from 20 to 55 °C) with a negative temperature coefficient of about 1%/K. This simplifying assumption seems sufficiently accurate, since temperature coefficient values calculated from Tables 1 and 2 range from 0.852 to 1.25%/K. Moreover, similar values may be inferred from experimental tests reported in [36].

To evaluate battery temperature T and the auxiliary consumptions (due to BMS and to the heating, ventilating, air conditioning, HVAC, system that controls the BESS cabinet temperature), a thermal model was set up and coupled to the equivalent electrical circuit [40]. Battery temperature depends on the balance between battery Joule losses $R_0(t) \cdot i(t)^2$ and thermal power removed by the HVAC:

$$\frac{dT}{dt} = \frac{R_0(t) \cdot i(t)^2 - \Delta T \cdot G}{C_T}, \tag{2}$$

where $\Delta T \cdot G$ is the thermal power removed by the HVAC (G is the thermal conductance, ΔT is the difference between battery temperature, T, and cabinet temperature T_0 set by HVAC) and C_T is the thermal capacitance of the battery. Thermal exchanges with the outside environment are neglected because of the extensive thermal insulation of the cabinet. Steady-state auxiliary consumptions are given by:

$$P_{aux} = \frac{R_0(t) \cdot i(t)^2}{COP} + P_{BMS}, \tag{3}$$

where COP is the HVAC coefficient of performance and P_{BMS} includes the power losses specifically related to the BMS (located outside the cabinet) and the power consumption due to PCS auxiliaries, assumed to be constant.

Values measured by Terna, i.e., G = 60 W/K, C_T = 100 Wh/K, T_0 = 20 °C, COP = 2.5 and P_{BMS} = 400 W, were used in simulations. Figure 6 shows the thermal and electrical power flows considered in the model.

4.2. Ageing Model

The ageing model proposed in [21] was adopted to represent the capacity loss (Q_{loss}) of the battery with charge-discharge cycles. The percentage Q_{loss} is given by:

$$Q_{loss} = B \cdot \exp\left(\frac{-31,700 + 370.3 \cdot (C\text{-}rate)}{8.314 \cdot T}\right) \cdot A_h^{0.55}, \tag{4}$$

where *C-rate* is the current charging/discharging rate, A_h is the accumulated charge throughput (Ah), expressed as (cycle number) × (*DOD*) × (full cell capacity), T is the absolute temperature (K) and B is a numerical factor depending on the *C-rate*. The model described by Equation (4) implicitly takes into account "calendar" (time) aging together with aging due to cycling, as long as the BESS is not idle; this condition is certainly fulfilled in the studied PFC application.

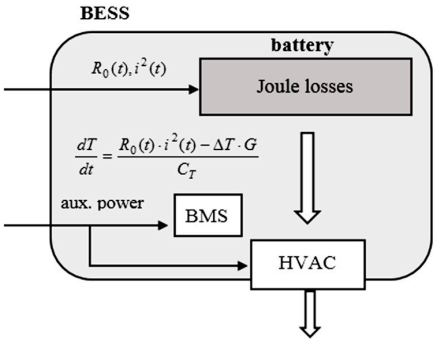

Figure 6. Thermal (white arrows) and electrical (black arrows) power flows associated to the BESS electrical-thermal model.

A power law least square approximation was carried out in order to evaluate B values corresponding to *C-rates* in the 0.005–6C range. B values reported in [21] for C/2, 2C and 6C, and a B value based on 20 years expected calendar life reported by the manufacturer for 0.005C (the latter is the lowest *C-rate* occurred during the simulations reported in this paper), were used. Such values are reported in Table 3. The resulting relationship is:

$$B = 26,222 \cdot (C\text{-}rate)^{-0.387}. \quad (5)$$

Table 3. B values used to calculate the *C-rate* vs. B power law approximation and obtained by Equation (5).

C-rate	*B*	*B* from Equation (5)
0.005C	207,000	203,781
C/2	31,630	34,290
2C	21,681	20,052
6C	12,934	13,108

Figure 7 reports the above data and the fitting power curve. End-of-life for the simulated battery is assumed when Q_{loss} equals 20% [22,23]. Figure 8 compares ageing model results with manufacturer's life cycle data, showing a very good agreement.

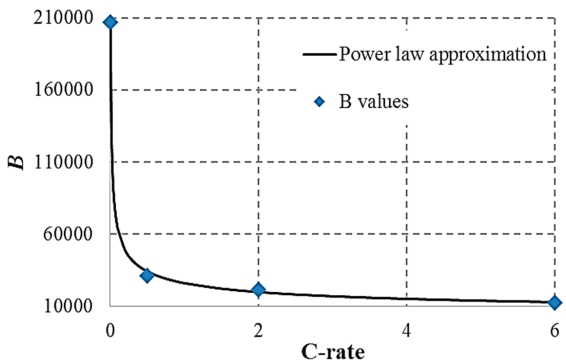

Figure 7. Experimental values [21] and fitting curve of B coefficient in the battery model (4), vs. *C-rate*.

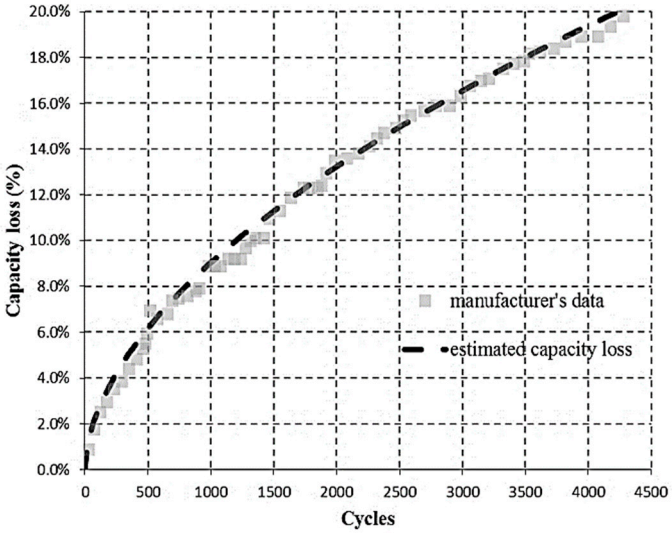

Figure 8. Capacity loss vs. number of cycles for the experimental $LiFePO_4$ battery string: comparison between cycle-life simulation model and experimental data from the manufacturer.

Manufacturer data reported in Figure 8 refer to complete charge-discharge cycles (*DOD* = 100%), with an average *C-rate* of 0.4C; the measured average battery temperature during each test cycle was T = 29 °C. Note that in this context (and throughout the paper) charge and discharge are calculated with reference to the commercial rating of the battery module, i.e., 185 Ah. The estimated capacity loss curve in Figure 8 has been computed by using (4), with T = 302.15 K, *C-rate* = 0.4, and B = 37,382.5 (as yielded by (5) with *C-rate* = 0.4).

5. Results of the Terna Experimental Primary Frequency Control Application

In this section, Terna experimental test results are reported and compared to simulations, in order to validate the electrical-thermal-ageing model presented in Section 4. The experimental test refers to a one-day period (i.e., 86,400 s), during which the battery string has been cycled by using the frequency profile described in Section 3.3, with a *C-rate* 1C and 0.5% droop. During the test, when the battery was completely discharged, PFC service was interrupted and the battery was completely re-charged (recharge time is 4 h), as in the actual operation of the Terna 1 MW/1 MWh BESS. This full recharge phase is mainly necessary in order to recalibrate the SOC estimation (performed by integrating the current flowing through the battery), which otherwise would be increasingly affected by the accumulation of measurement errors.

Figure 9a shows the comparison between measured and calculated battery string voltage during the one-day period, whereas in Figure 9b a zoom of the measured and calculated voltages in the time window between t = 13,000 s and t = 14,000 s is reported. Simulation results agree very well with measured results when the battery string is performing PFC, whereas substantial differences are evidenced during re-charging in Figure 9a, approximately from t = 47,000 s to t = 62,000 s. These differences are due to the lack of capacitances in the electrical model of the battery, which is more suitable for simulating PFC instead of continuative charge or discharge periods. The small differences between measured and calculated voltage shown in Figure 9b depend on small mismatches between actual and calculated SOC of the battery. The average error on voltage, calculated as:

$$V_{error,avg} = \frac{\sum_{i=1}^{N} \left| V_{calc,i} - V_{meas,i} \right|}{N}, \quad (6)$$

equals 6.09 V, i.e., less than 2.4% of rated string voltage.

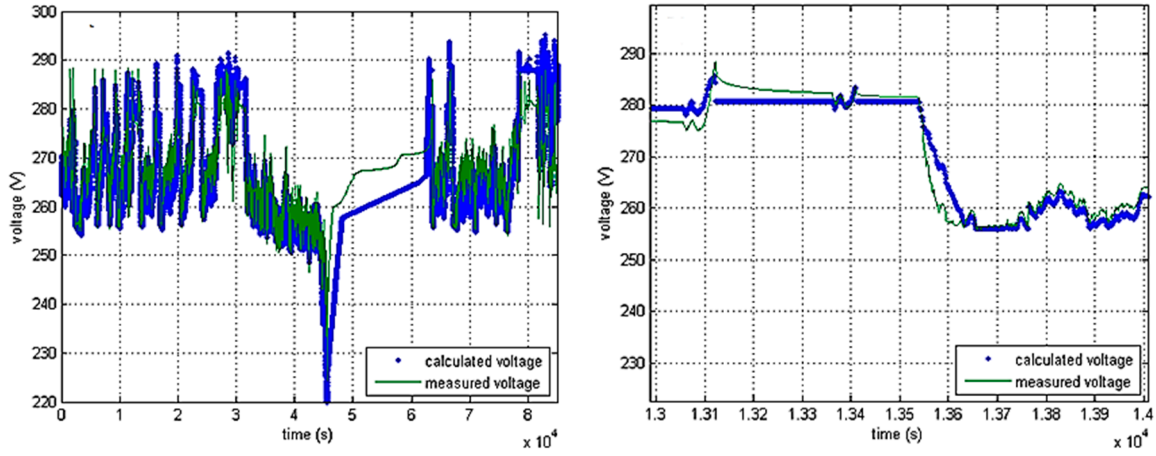

Figure 9. PFC tests, measured and calculated battery voltage vs. time: (**a**) voltage vs. time during 1 day; and (**b**) detail in the time range 13,000–14,000 s.

Figure 10a shows the comparison between measured and calculated battery string current during the one-day test period, whereas Figure 10b details the time window between t = 13,000 s and t = 14,000 s. Both figures show a very good agreement: the average error on current is 3.63 A, i.e., 2% of rated current.

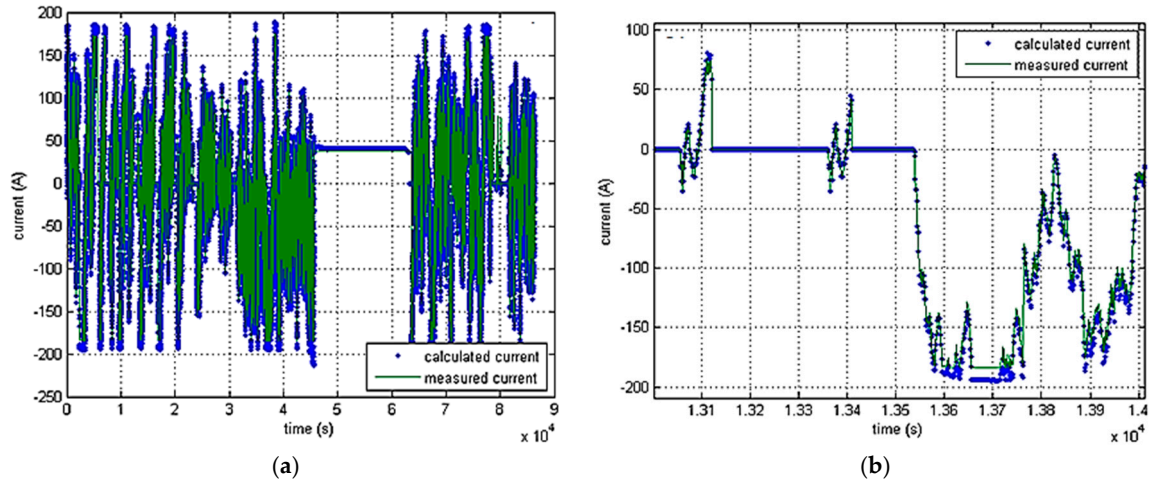

Figure 10. PFC tests, measured and calculated battery current vs. time: (**a**) current vs. time during 1 day; and (**b**) detail in the time range 13,000–14,000 s.

Lastly, Figure 11 reports the measured and calculated battery mean temperature T_m (i.e., the average between the temperatures of each cell in the battery string); the measured "ambient" temperature in the cabinet T_0 (i.e., the temperature imposed by the HVAC) is also shown. Measured and calculated values of T_m are in acceptable agreement, whereas the measured T_0 is always very close to the target value T_0 = 20 °C, thus confirming the approximation made in Equation (2), where ΔT is calculated considering a constant T_0.

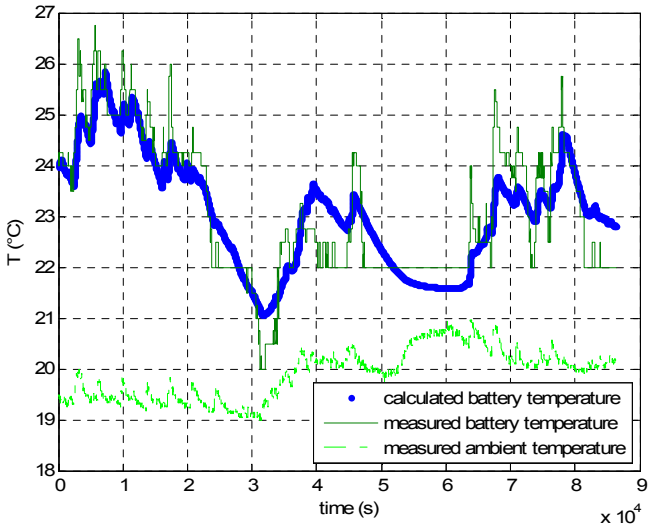

Figure 11. PFC tests, measured and calculated battery mean temperature T_m, and measured ambient (cabinet) temperature T_0, vs. time.

6. Primary Frequency Control Simulation Results

PFC simulations were carried out on a 50 kWh $LiFePO_4$ battery: since the BESSs is modular, results can be easily scaled to other BESS sizes. PFC operation of the 50 kWh battery was simulated for seven different droop values, namely 0.075%, 0.1%, 0.25%, 0.5%, 1%, 2% and 4%, and four different *C-rate* values, i.e., C/2, 1C, 2C and 4C, considering in all cases the frequency profile described in Section 3.3. Battery performance was evaluated in terms of:

- Average number of charge-discharge cycles per day;
- Overall battery efficiency η_{TOT}, including auxiliary consumptions calculated with (3) and assuming 96% PCS efficiency [26];
- Mean temperature, T_m, of the battery in operation (maximum allowed battery temperature T_{max} is 55 °C);
- Mean *C-rate* during the whole operation;
- Battery power-frequency characteristic λ (kW/Hz);
- Expected life;
- Unavailability of the battery rack for the PFC service (due to SOC outside the operating range or T_m exceeding the maximum temperature T_{max} = 55 °C), in percent of the overall operation time.

Results are summarized in Tables 4–7. These also include the equivalent power-frequency characteristic λ (kW/Hz), calculated from rated energy W_{rated} (kWh), *C-rate* and droop *s*:

$$\lambda = \frac{C{-}rate \cdot W_{rated}}{f_n} \cdot \frac{100}{s}. \quad (7)$$

Table 4. PFC results: *C-rate* = C/2, T_0 = 20 °C.

s (%)	Cycles per Day	η_{Tot} (%)	T_m (°C)	Mean *C-rate*	λ (kW/Hz)	Life (Years)	Not Operated (%)
0.075	2.51	82.35	21.7	0.21	666.7	5.43	0
0.1	2.03	81.07	21.3	0.17	500	6.03	0
0.25	0.92	72.65	20.4	0.08	200	8.31	0
0.5	0.47	59.67	20.2	0.04	100	10.48	0
1	0.24	41.54	20.1	0.02	50	13.05	0
2	0.12	22.44	20.1	0.01	25	16.07	0
4	0.06	9.31	20.0	0.005	12.5	20	0

Table 5. PFC results: *C-rate* = 1C, T_0 = 20 °C.

s (%)	Cycles per Day	η_{Tot} (%)	T_m (°C)	Mean *C-rate*	λ (kW/Hz)	Life (Years)	Not Operated (%)
0.075	5.09	83.28	27.0	0.42	1333	2.76	4.6
0.1	4.24	82.95	25.5	0.35	1000	3.33	4.6
0.25	1.85	79.31	21.7	0.15	400	6.10	0
0.5	0.94	72.10	20.7	0.08	200	8.11	0
1	0.47	59.55	20.3	0.04	100	10.40	0
2	0.24	41.50	20.1	0.02	50	13.05	0
4	0.12	22.40	20.1	0.01	25	16.07	0

Table 6. PFC results: *C-rate* = 2C, T_0 = 20 °C.

s (%)	Cycles per Day	η_{Tot} (%)	T_m (°C)	Mean *C-rate*	λ (kW/Hz)	Life (Years)	Not Operated (%)
0.075	8.86	79.90	43.9	0.74	2667	0.63	11.1
0.1	7.54	80.41	38.6	0.63	2000	0.99	4.1
0.25	4.14	80.02	28.7	0.34	800	2.64	2.3
0.5	1.88	77.68	22.7	0.16	400	5.51	0
1	0.95	71.04	21.1	0.08	200	7.85	0
2	0.48	59.00	20.4	0.04	100	10.31	0
4	0.24	41.29	20.2	0.02	50	12.94	0

Table 7. PFC results: *C-rate* = 4C, T_0 = 20 °C.

s (%)	Cycles per Day	η_{Tot} (%)	T_m (°C)	Mean *C-rate*	λ (kW/Hz)	Life (Years)	Not Operated (%)
0.075	7.55	72.72	54.5	0.63	5333	0.34	54
0.1	7.73	73.26	54.3	0.64	4000	0.40	48.3
0.25	5.88	75.11	42.2	0.49	1600	0.86	15.5
0.5	3.78	76.73	31.1	0.31	800	2.28	0
1	1.91	74.85	24.5	0.16	400	4.78	0
2	0.96	69.43	21.7	0.08	200	7.49	0
4	0.48	58.30	20.6	0.04	100	10.15	0

Data in Tables 4–7 are re-arranged in graphical form as Figures 12 and 13. Figure 12a plots the overall efficiency vs. expected battery life for different droop values, whereas in Figure 12b curves of efficiency vs. expected life are shown for different *C-rate* values.

Figure 12 shows that PFC operation with low droop values results in a good overall efficiency, even exceeding 80% as shown in Figure 12a, especially with the lower simulated *C-rate* values as shown in Figure 12b. Higher efficiencies, however, are traded with expected life values much shorter than the 20 years conventional BESS calendar life, because very low droops are associated to more sustained cycling. This is the limiting factor on efficiency for the extreme simulated combinations of low droop and high *C-rate*, which are also associated to the onset of operating constraints such as battery overtemperature and SOC limits, which limit battery utilization. Conversely, low *C-rates* combined with higher droop result in much longer battery expected life, at the expense of a sharp decrease in overall efficiency η_{TOT} due to low battery utilization.

Efficiency and expected life values from Tables 4–7 are plotted in Figure 13 as a function of the equivalent power-frequency characteristic λ. Figure 13 shows that combinations of droop and *C-rate* yielding the same λ largely result in similar lifetimes and efficiencies, so that battery power-frequency characteristic could be taken as the actual design parameter for performing PFC with a BESS. As long as the system is linear and time-invariant, the same λ values lead to the same results. However, both the model and the control strategy (which includes dead band, recharge phase, temperature and SOC limits) are not linear, resulting in some differences.

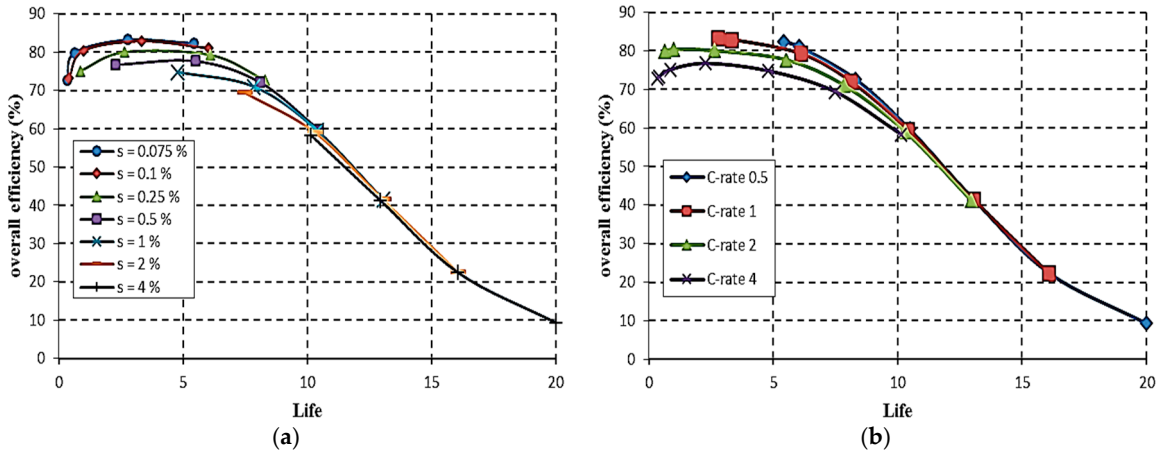

Figure 12. Overall efficiency vs. expected life: (**a**) as a function of droop; (**b**) as a function of *C-rate*.

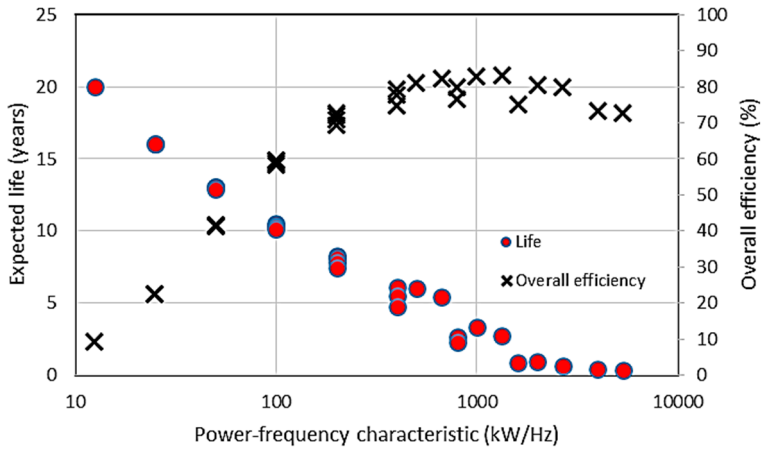

Figure 13. Expected battery life and overall efficiency vs. power-frequency characteristic.

Such differences are smaller when the battery is less stressed (i.e., at low λ values), and increase with increasing λ values. It should be pointed out that the longer BESS lifetimes predicted at low λ values could be offset by components having a shorter life than the battery itself, notably the electronic equipment.

To carry out an economic evaluation of the PFC application, applicable (i.e., national) rules of the electric energy market must be considered, assuming that a PFC market exists. Considering the different national approaches and the relative volatility of the regulatory framework for ancillary services, only general economic remarks can be made here.

Notably, given the short BESS lifetime under intensive cycling, the most favorable scenario would seem to be a capacity-based PFC market (especially in association to high *C-rate* values), whereas operation in an energy-based PFC market, such as in Italy [41], seems much less promising due to need for sustained cycling. Taking the capacity-based German PFC market as the reference market, some rough net present values (*NPV*) calculations may be made for the Terna's 1 MWh BESS. Since such a market remunerates primary control for each MW of reserve deployed when Δf = 200 mHz [42,43], s = 0.4% is the droop value required in order to fully exploit the 1 MWh BESS for PFC (Equation (1)). Table 8 reports PFC results obtained for s = 0.4% and for different *C-rate* values.

Table 8. PFC results for s = 0.4%, T_0 = 20 °C.

C-rate	Cycles per Day	η_{Tot} (%)	T_m (°C)	Mean *C-rate*	λ (kW/Hz)	Life (Years)	Not Operated (%)
0.5	0.58	59.66	20.3	0.05	125	9.8	0
1	1.17	71.85	21.0	0.1	250	7.44	0
2	2.34	77.04	23.8	0.20	500	4.70	0
4 [(1)]	4.57	75.31	35.1	0.38	1000	1.57	1.5

[(1)] *C-rate* values higher than 2C could be allowable in the next future if the 30-min criterion (actually adopted in the German PFC market) is relaxed to 15-min criterion.

Figure 14 reports *NPV*s, calculated for s = 0.4%, as a function of *C-rate*. A 3.6% capitalization factor and a 20-year BESS operation period have been considered. With reference to recent Terna BESS projects [24,44], battery cost has been set to 0.4 M€/MWh (if the battery life is shorter than 20 years, replacement cost is accounted as yearly economic losses equal to the ratio between battery cost and estimated battery life); fixed costs (civil works, MV switchgear, control system) have been set to 0.8 M€/MWh; PCS cost has been considered to be 0.2 M€/MW. The cost of losses, which are evaluated by means of the overall efficiency η_{TOT}, has been set at 140 €/MWh, whereas weekly revenues have been set to $R_{w,unitary}$ = 3000 €/MW/week, a typical value for the German market [45]. For the same 1 MWh battery, consideration of different nominal *C-rates* (namely 0.5C, 1C, 2C and 4C) leads to different unitary BESS active power capabilities (0.5 MW, 1 MW, 2 MW and 4 MW, respectively). As a consequence, the weekly revenues (which depends on BESS active power capability) linearly depend on *C-rates*. The yearly incomes $R_{y,tot}$ have thus been evaluated as:

$$R_{y,tot} = \frac{365}{7} \cdot R_{w,unitary} \cdot C{-}rate. \quad (8)$$

Due to the modular design of BESS [24], this implies that the economic evaluation for a larger system could be simply carried out by scaling up the above-described implementation and its attendant costs and revenues.

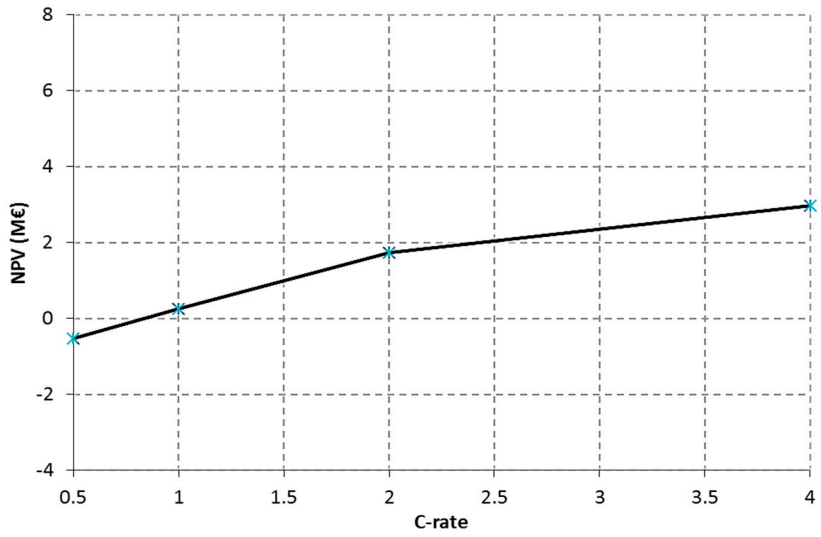

Figure 14. Estimated *NPV* for a 1 MWh BESS, for different *C-rates* (0.4% droop, capacity-based PFC market).

7. Conclusions

The paper studied the application of a $LiFePO_4$ BESS to primary frequency control, in the ENTSO-E Continental Europe grid; technical data from Terna's (the Italian TSO) experimental system has been used for defining BESS characteristics. BESS behavior has been simulated by the combination

of an electrical-thermal circuit model with a life-cycle model predicting the capacity loss of the $LiFePO_4$ battery due to charge-discharge cycles. The complete electrical-thermal-ageing model has been subsequently validated by comparisons both with experimental tests carried out by Terna and with manufacturer data. Lastly, numerical PFC simulations have been performed by using actual Italian (ENTSO-E continental system) frequency recordings and considering a conventional, proportional "governor" for the BESS, for a wide range of different droop/*C-rate* combinations.

The main result evidenced by the simulations is that high overall BESS efficiency and expected lifetime are conflicting requirements. High efficiency in PFC service is associated to *C-rate*/droop combinations yielding high values of the power-frequency characteristic λ, which naturally results in sustained cycling of the BESS that drastically shortens expected battery lifetime. As an example, for the simulated and tested 50 kW-50 kWh battery string the choice of λ = 200 kW/Hz (*C-rate* = 1C, 0.5% droop) results in an overall efficiency exceeding 72%, but the expected lifetime is about 8 years. For a given frequency profile, lower λ values (e.g., associated to the usual 4%–5% droop of conventional generators' governors) result in less battery cycling and longer lifetimes, possibly approaching the conventional 20 years value, albeit with much lower efficiencies due to auxiliary losses.

The paper showed the technical feasibility of $LiFePO_4$ BESS use in primary frequency control, evidencing that there is a significant trade-off between expected lifetime and overall efficiency, restricting the choice of operating parameters to a rather narrow band; in the studied system, lifetimes in excess of 10 years are actually associated to efficiencies below 60%, mainly because of BESS underutilization.

Besides the above reported technical issues, an economic evaluation would depend on the specific (national) rules of the PFC market, whether capacity-based or energy-based. Considering a capacity–based market, such as the German one, results show that high *C-rate* values ($\geq$1C) seem to be more profitable.

Author Contributions: Terna S.p.A. (Massimo Rebolini and Francesco Palone) conceived, designed and commissioned the experiments; Francesco Palone and Marco Maccioni analyzed the data; Francesco Palone, Marco Maccioni, Alberto Geri, Fabio Massimo Gatta, Stefano Lauria, Regina Lamedica and Alessandro Ruvio wrote the paper.

Conflicts of Interest: The authors declare no conflict of interest.

References

1. Yang, Y.; Li, H.; Aichhorn, A.; Zheng, J.; Greenleaf, M. Sizing strategy of distributed battery storage system with high penetration of photovoltaic for voltage regulation and peak load shaving. *IEEE Trans. Smart Grid* **2014**, *5*, 982–991. [CrossRef]
2. Choi, J.H.; Kim, J.C. Advanced voltage regulation method of power distribution systems interconnected with dispersed storage and generation systems. *IEEE Trans. Power Deliv.* **2001**, *16*, 329–334. [CrossRef]
3. Cresta, M.; Gatta, F.M.; Geri, A.; Maccioni, M.; Mantineo, A.; Paulucci, M. Optimal operation of a LV distribution network with renewable DG by NaS battery and demand response strategy: A case study in a trial site. *IET Renew. Power Gen.* **2015**, *9*, 549–556. [CrossRef]
4. Borsche, T.; Ulbig, A.; Koller, M.; Andersson, G. Power and energy capacity requirements of storages providing frequency control reserves. In Proceedings of the 2013 IEEE Power and Energy Society General Meeting, Vancouver, BC, Canada, 21–25 July 2013.
5. Mégel, O.; Mathieu, J.L.; Andersson, G. Maximizing the potential of energy storage to provide fast frequency control. In Proceedings of the 4th IEEE Power and Energy Society Innovative Smart Grid Technologies Europe (ISGT Europe 2013), Copenhagen, Denmark, 6–9 October 2013.
6. Oudalov, A.; Chartouni, D.; Ohler, C. Optimizing a battery energy storage system for primary frequency control. *IEEE Trans. Power Syst.* **2007**, *22*, 1259–1266. [CrossRef]
7. Falvo, M.C.; Lamedica, R.; Bartoni, R.; Maranzano, G. Energy saving in metro-transit systems: Impact of braking energy management. In Proceedings of the 2010 IEEE International Symposium on Power Electronics, Electrical Drives, Automation and Motion (SPEEDAM 2010), Pisa, Italy, 14–16 June 2010.

8. Falvo, M.C.; Lamedica, R.; Ruvio, A. An environmental sustainable transport system: A trolley-buses line for Cosenza city. In Proceedings of the 2012 IEEE International Symposium on Power Electronics, Electrical Drives, Automation and Motion (SPEEDAM 2012), Sorrento, Italy, 20–22 June 2012.
9. Falvo, M.C.; Lamedica, R.; Ruvio, A. Energy storage application in trolley-buses lines for a sustainable urban mobility. In Proceedings of the 2012 IEEE International Symposium on Electrical Systems for Aircraft, Railway and Ship Propulsion (ESARS 2012), Bologna, Italy, 16–18 October 2012.
10. Calderaro, V.; Galdi, V.; Graber, G.; Piccolo, A. Siting and sizing of stationary supercapacitors in a metro network. In Proceedings of the 2013 AEIT Annual Conference, Mondello, Italy, 3–5 October 2013.
11. Barton, J.; Infield, D. Energy storage and its use with intermittent renewable energy. *IEEE Trans. Energy Convers.* **2004**, *19*, 441–448. [CrossRef]
12. Schainker, R. Executive overview: Energy storage options for a sustainable energy future. In Proceedings of the IEEE Power Engineering Society General Meeting, Denver, CO, USA, 6–10 June 2004.
13. Leonhard, W.; Grobe, E. Sustainable electrical energy supply with wind and pumped storage—A realistic long-term strategy or Utopia? In Proceedings of the IEEE Power Engineering Society General Meeting, Denver, CO, USA, 6–10 June 2004.
14. Meneses de Quevedo, P.; Contreras, J. Optimal placement of energy storage and wind power under uncertainty. *Energies* **2016**, *9*, 528. [CrossRef]
15. Grasselli, U.; Lamedica, R.; Prudenzi, A. Time-varying harmonics of single-phase non-linear appliances. In Proceedings of the IEEE Power Engineering Society Winter Meeting, New York, NY, USA, 27–31 January 2002.
16. Lamedica, R.; Maranzano, G.; Marzinotto, M.; Prudenzi, A. Power quality disturbances in power supply system of the subway of Rome. In Proceedings of the IEEE Power Engineering Society General Meeting, Denver, CO, USA, 6–10 June 2004.
17. Lamedica, R.; Marzinotto, M.; Prudenzi, A. Harmonic amplitudes and harmonic phase angles monitored in an electrified subway system during rush-hours traffic. In Proceeding of International Conference on Applied Simulation and Modelling (IASTED 2004), Rhodes, Greece, 28–30 June 2004.
18. Falvo, M.C.; Grasselli, U.; Lamedica, R.; Prudenzi, A. Harmonics monitoring survey on office LV appliances. In Proceedings of the 14th International Conference on Harmonics and Quality of Power (ICHQP 2010), Bergamo, Italy, 26–29 September 2010.
19. BYD Company. Available online: http://www.byd.com/energy/reference_ess.htm (accessed on 27 October 2016).
20. A123 Systems to Supply 20MW of Advanced Energy Storage Solutions to AES Gener for Spinning Reserve Project in Chile. Available online: http://www.a123systems.com/ca93980e-389a-40c6-86f9-b869feabe908/media-room-2011-press-releases-detail.htm (accessed on 27 October 2016).
21. Wang, J.; Liu, P.; Hicks-Garner, J.; Shermana, E.; Soukiazia, S.; Verbrugge, M.; Tataria, H.; Musser, J.; Finamore, P. Cycle-life model for graphite-$LiFePO_4$ cells. *J. Power Sources* **2011**, *196*, 3942–3948. [CrossRef]
22. Swierczynski, M.; Stroe, D.I.; Stan, A.I.; Teodorescu, R. Primary frequency regulation with Li-ion battery energy storage system: A case study for Denmark. In Proceedings of the 5th IEEE Annual International Energy Conversion Congress and Exhibition, Melbourne, Australia, 3–6 June 2013; pp. 487–492.
23. Swierczynski, M.; Stroe, D.I.; Stan, A.I.; Teodorescu, R.; Sauer, D.U. Selection and performance-degradation modeling of $LiMO_2/Li_4Ti_5O_{12}$ and $LiFePO_4$/C battery cells as suitable energy storage systems for grid integration with wind power plants: An example for the primary frequency regulation service. *IEEE Trans. Sustain. Energy* **2014**, *5*, 90–101. [CrossRef]
24. Alì, A.; Gionco, S.; Palone, F.; Rebolini, M.; Polito, R. Sistemi di automazione e soluzioni impiantistiche per i sistemi di accumulo elettrochimici per la rete di trasmissione nazionale. *L'Energia Elettr.* **2014**, *91*, 71–84. (In Italian)
25. Tortora, A.C.; Senatore, E.; Apicella, L.; Polito, R. Sistemi di accumulo di energia elettrochimici per la gestione efficiente delle fonti rinnovabili non programmabili. *L'Energia Elettr.* **2014**, *91*, 35–46. (In Italian)
26. Andriollo, A.; Benato, R.; Bressan, M.; Dambone Sessa, S.; Palone, F.; Polito, R.M. Review of power conversion and conditioning systems for stationary electrochemical storage. *Energies* **2015**, *8*, 960–975. [CrossRef]
27. *Secondary Cells and Batteries Containing Alkaline or Other Non-Acid Electrolytes—Safety Requirements for Portable Sealed Secondary Cells, and for Batteries Made from Them, for Use in Portable Applications*, 2.0 ed.; IEC 62133; International Electrotechnical Commission (IEC): Geneva, Switzerland, 2012.

28. *Safety of Primary and Secondary Lithium Cells and Batteries during Transport*, 2.0 ed.; IEC 62281; International Electrotechnical Commission (IEC): Geneva, Switzerland, 2012.
29. Gatta, F.M.; Geri, A.; Lauria, S.; Maccioni, M.; Palone, F. Arc-flash in large battery energy storage systems—Hazard calculation and mitigation. In Proceedings of the 16th IEEE International on Environment and Electrical Engineering (EEEIC 2016), Florence, Italy, 7–10 June 2016.
30. Künisch, H.J.; Krämer, K.G.; Dominik, H. Battery energy storage another option for load-frequency-control and instantaneous reserve. *IEEE Trans. Energy Convers.* **1986**, *1*, 41–46. [CrossRef]
31. Koller, M.; Borsche, T.; Ulbig, A.; Andersson, G. Review of grid applications with the Zurich 1 MW battery energystorage system. *Electr. Power Syst. Res.* **2015**, *120*, 128–135. [CrossRef]
32. Department of Energy, DoE, Global Energy Storage Database. Available online: http://www.energystorageexchange.org/projects (accessed on 27 October 2016).
33. UCTE Continental Europe Operation Handbook. Available online: https://www.entsoe.eu/publications/system-operations-reports/operation-handbook/Pages/default.aspx (accessed on 27 October 2016).
34. Terna Rete Italia, 'Partecipazione Alla Regolazione di Frequenza e Frequenza-Potenza' (2008). Available online: http://download.terna.it/terna/0000/0105/32.pdf (accessed on 27 October 2016).
35. Terna Rete Italia, 'Qualità del Servizio di Trasmissione Rapporto Annuale per L'anno 2014' (2014). Available online: http://download.terna.it/terna/0000/0108/85.pdf (accessed on 27 October 2016).
36. Ke, M.Y.; Chiu, Y.H.; Wu, C.Y. Battery modelling and SOC estimation of a $LiFePO_4$ battery. In Proceedings of the 2016 International Symposium on Computer, Consumer and Control (IS3C 2016), Xi'an, China, 4–6 July 2016.
37. Huria, T.; Ceraolo, M.; Gazzarri, J.; Jackey, R. High fidelity electrical model with thermal dependence for characterization and simulation of high power lithium battery cells. In Proceeding of the 2012 IEEE International Electric Vehicle Conference (IEVC 2012), Greenville, SC, USA, 4–8 March 2012.
38. Waag, W.; Kabitz, S.; Sauer, D.U. Experimental investigation of the lithium-ion battery impedance characteristic at various conditions and aging states and its influence on the application. *Appl. Energy* **2013**, *102*, 885–897. [CrossRef]
39. Stroe, D.; Swierczynski, M.; Stan, A.I.; Teodorescu, R.; Andreasen, S.J. Experimental investigation on the internal resistance of Lithium iron phosphate battery cells during calendar ageing. In Proceedings of the 39th Annual Conference of the IEEE Industrial Electronics Society (IECON 2013), Vienna, Austria, 10–14 November 2013.
40. Gatta, F.M.; Geri, A.; Lauria, S.; Maccioni, M.; Palone, F. Battery energy storage efficiency calculation including auxiliary losses: Technology comparison and operating strategies. In Proceedings of the 2015 IEEE Powertech, Eindhoven, The Netherlands, 29 June–2 July 2015.
41. Specifiche tecniche per la verifica e valorizzazione del servizio di regolazione primaria di frequenza (2014). Available online: http://download.terna.it/terna/0000/0105/89.pdf (accessed on 27 October 2016). (In Italian)
42. Eckpunkte und Freiheitsgrade bei Erbringung von Primärregelleistung—Leitfaden für Anbieter von Primärregelleistung. Available online: https://www.regelleistung.net/ext/download/eckpunktePRL (accessed on 27 October 2016).
43. Zeh, A.; Müller, M.; Naumann, M.; Hesse, H.C.; Jossen, A.; Witzmann, R. Fundamentals of using battery energy storage systems to provide primary control reserves in Germany. *Batteries* **2016**, *2*, 29. [CrossRef]
44. Terna Open Construction Sites. Available online: http://www.terna.it/en-gb/cantieriapertitrasparenti.aspx (accessed on 27 October 2016).
45. Primary Control Reserve Tender Results. Available online: https://www.regelleistung.net (accessed on 27 October 2016).